JOURNAL
OF
MICROBIOLOGY
AND
BIOTECHNOLOGY

© The Korean Society for Microbiology and Biotechnology

Functional Roles of the Aromatic Residues in the Stabilization of the [Fe₄S₄] Cluster in the Iro Protein from *Acidithiobacillus ferrooxidans*

Zeng, Jia[1]*, Qing Liu[2], Xiaojian Zhang[2], Hongyu Mo[2], Yiping Wang[2], Qian Chen[2], and Yuandong Liu[2]

[1]*Center for Biomedical Engineering, State Key Laboratory of Chemo/Biosensing and Chemometrics, Hunan University, Changsha, Hunan 410082, P. R. China*
[2]*Department of Bioengineering, Central South University, Changsha, Hunan 410083, P. R. China*

The Iro protein is a member of the HiPIP family with the [Fe₄S₄] cluster for electron transfer. Many reports proposed that the conserved aromatic residues might be responsible for the stability of the iron–sulfur cluster in HiPIP. In this study, Tyr10 was found to be a critical residue for the stability of the [Fe₄S₄] cluster, according to site-directed mutagenesis results. Tyr10, Phe26, and Phe48 were essential for the stability of the [Fe₄S₄] cluster under acidic condition. Trp44 was not involved in the stability of the [Fe₄S₄] cluster. Molecular structure modeling for the mutant Tyr10 proteins revealed that the aromatic group of Tyr10 may form a hydrophobic barrier to protect the [Fe₄S₄] cluster from solvent.

Keywords: *Acidithiobacillus ferrooxidans*, Iro protein, iron–sulfur cluster, mutation, molecular modeling.

Acidithiobacillus ferrooxidans is an acidophilic chemolithotrophic bacterium, which obtains energy by oxidation of ferrous iron to ferric iron [13]. The electron transfer cycle for the iron oxidation in *Acidithiobacillus ferrooxidans* include four steps. First, ferrous ion is oxidized by the Iro protein, and the reduced Iro protein then transfers electrons to cytochrome $c552$. In the third step, cytochrome $c552$ transfers electrons to a cytochrome c oxidase, and finally, electrons are transferred to molecular oxygen by the oxidase [16].

The Iro protein is a member of the high redox potential iron–sulfur proteins (HiPIP) [4, 5, 8]. The HiPIP is a class of small proteins (6–10 kDa) containing a [Fe₄S₄] cluster per monomer. This cluster is known to perform a wide range of functions, including electron transfer, substrate recognition, and sensing or regulatory functions. The iron–sulfur center undergoes one-electron reactions between

$[Fe_4S_4]^{2+}$ and $[Fe_4S_4]^{3+}$ with redox potentials ranging from +50 to +450 mV.

Many reports proposed that the conserved aromatic residues might be responsible for the stability of the iron–sulfur cluster in HiPIP [2, 7, 11, 12, 14]. It was reported that both Tyr19 of *C. vinosum* HiPIP and Tyr12 of *Ectothiorhodospira halophila* HiPIP play critical roles in the stability of the cluster, and polar residue substitutions of the tyrosine residue resulted in significant instability of the [Fe₄S₄] cluster [1, 6]. Sequences alignment of Iro protein from *A. ferrooxidans* and HiPIPs from various sources showed that Tyr10, Phe26, Trp44, and Phe48 are conserved residues, as shown in Fig. 1. These aromatic residues might play important roles in stabilizing the iron–sulfur cluster. In this study, Tyr10 was found to be crucial for the stability of the [Fe₄S₄] cluster, according to site-directed mutagenesis results. Tyr10, Phe26, and Phe48 were essential for maintaining the stability of the [Fe₄S₄] cluster under acidic conditions. Trp44 was not essential for the stability of the [Fe₄S₄] cluster. Molecular modeling for mutant Tyr10 proteins revealed that the aromatic group of Tyr10 protected the [Fe₄S₄] cluster from solvent.

MATERIALS AND METHODS

Materials

A HiTrap chelating metal affinity column was purchased from GE healthcare Ltd. TOP10 competent cells and *E. coli* strain BL21(DE3) competent cells came from Invitrogen Life Technologies. The Plasmid Mini kit, a gel extraction kit, and synthesized oligonucleotides were obtained from Sangon Company of Shanghai. pfu DNA polymerase and restriction enzymes came from MBI Fermentas of Germany. All other reagents were of research grade or better and obtained from commercial sources.

Construction of the Mutant Plasmids of the Iro Protein

A QuikChange mutagenesis kit (Stratagene) was applied for constructing the mutant expression plasmids. The plasmid pLM1::IRO was used

*Corresponding author
Phone: +86 731 88821740; Fax: +86 731 88821740;
E-mail: zengjcsu@yahoo.com.cn

```
Iro    ----------GSMPKAAVQYQDTPK--------------GKDHCSVCAQFI------- 27
Hip    PIGAAHAAGNCPGTTPKAEVQYQPHPK-------------GKDQCSVCANFI------- 39
T. t   --AAPAN-AVTADDPTAIALKYNQDATKSERVAAARPGLPPEEQHCANCQFMQANVG--E 55
C. v   --SAPAN-AVAADDATAIALKYNQDATKSERVAAARPGLPPEEQHCANCQFMQADAAGAT 57
C. p   ---VPAN-AVTESDPAAVALKYHRDAASSERVAAARPGLPPEEQHCENCQFMNPDSA--A 54
E. h   --GLPDGVEDLPKAEDDHAHDYVNDAADTDHARFQ-----EGGLCENCQFWVDYVN--- 49
R. g   ----------QDKIDPKMVQYQDSPK-------------DGNKCSTCVNFE------- 28
R. t   -------G--TNASMRKAFNYQEVSKT-------------AGKNCANCAQFIPGAS--A 35
                        . *  .              . * *
```

```
Iro    -APHSCKV--VAG--NISPNGWCVAFVPKSA---- 53
Hip    -APKCCKV--VAG--PVAPDGYCIAFTPMPA---- 65
T. t   GDWKGCQL--FPG-KLINVNGWCASWTLKAG---- 83
C. v   DEWKGCQL--FPG-KLINVNGWCASWTLKAG---- 85
C. p   ADWKGCQL--FPG-KLINLSGWCASWTLRAG---- 82
E. h   -GWGYCQHPDFTD-VLVRGEGWCSVYAPA------ 76
R. g   -APSSCKI--VAG--KISPNGWCIAYAPMEDKKG- 57
R. t   SAAGACKV--IPGDSQIQPTGYCDAYIVKK----- 63
               *      : *:*  :
```

Fig. 1. Sequences alignment of Iro protein from *A. ferrooxidans* and HiPIPs from various sources.

Iro: Iro protein from *A. ferrooxidans* Fe; Hip: HiPIP from *A. ferrooxidans* 23270; T.t: HiPIP from *Thermochromatium tepidum*; C.v: HiPIP from *Chromatium vinosum*; C.p: HiPIP from *Chromatium purpuratum*; E.h: HiPIP from *Ectothiorhodospira halophila*; R.g: HiPIP from *Rhodopila globiformis*; R.t: HiPIP from *Rhodocyclus tenuis*. Residues conserved in all sequences are marked with *. Residues not conserved in all sequences but conserved in some sequences are marked with : or . based on the degree of conservation.

as a template for constructing mutant expression plasmids through PCR [17]. The primers and their antisense primers were synthesized to introduce the mutated sequence, as shown in Table 1.

PCR amplification was performed using *Pfu* DNA polymerase and samples were subjected to 13 cycles of 0.5 min of denaturation at 95°C, 1 min of annealing at 61°C, and 12 min of elongation at 72°C. The constructed mutant plasmids were transformed into TOP10 competent cells for screening purposes. Mutant expression plasmids of pIRO(Y10A), pIRO(Y10E), pIRO(Y10F), pIRO(Y10S) pIRO(Y10W), pIRO(F26A), pIRO(F26S), pIRO(F26W), pIRO(F26Y), pIRO(W44A),

pIRO(W44F), pIRO(W44S), pIRO(W44Y), pIRO(F48A), pIRO(F48S), pIRO(F48W), and pIRO(F48Y) were successfully constructed, and their sequences were verified by DNA sequencing. The mutant expression plasmids were transformed into *E. coli* BL21(DE3) for expression.

Expression and Purification of the Mutant Proteins

Expression and purification procedures for the Iro mutant proteins were identical to that of wild-type Iro protein [17]. The method of Bradford [3] was used to determine the protein content with bovine serum albumin as the standard. The purified mutant proteins were analyzed by SDS–polyacrylamide gel electrophoresis (SDS–PAGE) with 15% of acrylamide according to Laemmli [9].

Circular Dichroism Spectroscopy

Circular dichroism (CD) spectroscopy was carried out at 25°C using a Jasco J810 spectropolarimeter. The far-UV spectra of the proteins were measured from 190 to 260 nm in 20 mM potassium phosphate buffer, pH 7.4. Instrument settings: response 1 s, speed 50 nm/min, an average of four scans, and path length 1 mm. The data were processed by subtracting the buffer spectrum.

UV–Vis Scanning and EPR Spectra

UV–visible spectra scanning was carried out at 25°C on a Techcomp UV-2300 spectrophotometer. The samples of reduced and oxidized Iro proteins (10 µM) were prepared in 20 mM phosphate buffer containing 0.5 M NaCl, pH 7.4. X-Band EPR spectra were recorded at 70 K on a JEOL JES-FE1XG spectrometer. Parameters for recording the EPR spectra were typically 15–30 mT/min sweep rate, 0.63 mT modulation amplitude, 9.14 GHz frequency, and 4 mW incident microwave power, and the sweep time was 2 min. The samples were diluted to 5 µM in 20 mM phosphate buffer containing 0.5 M NaCl, pH 7.4. The oxidized Iro protein was obtained by incubating with 5 mM ammonium persulfate for 30 min.

Table 1. Primers designed for creating mutants.

Variant	Primer
Y10A	5'-AGGCAGCGGTGCAAGCTCAGGATACACCTA-3'
Y10E	5'-AGGCAGCGGTGCAAGAACAGGATACACCTA-3'
Y10F	5'-AGGCAGCGGTGCAATTTCAGGATACACCTA-3'
Y10S	5'-AGGCAGCGGTGCAATCTCAGGATACACCTA-3'
Y10W	5'-AGGCAGCGGTGCAATGGCAGGATACACCTA-3'
F26A	5'-CAGTCTGTGCGCAGGCTATTGCTCCACATA-3'
F26S	5'-CAGTCTGTGCGCAGTCTATTGCTCCACATA-3'
F26W	5'-CAGTCTGTGCGCAGTGGATTGCTCCACATA-3'
F26Y	5'-CAGTCTGTGCGCAGTATATTGCTCCACATA-3'
W44A	5'-TCAGCCCCAATGGCGCGTGTGTAGCCTTTG-3'
W44F	5'-TCAGCCCCAATGGCTTTTGTGTAGCCTTTG-3'
W44S	5'-TCAGCCCCAATGGCTCTTGTGTAGCCTTTG-3'
W44Y	5'-TCAGCCCCAATGGCTATTGTGTAGCCTTTG-3'
F48A	5'-GCTGGTGTGTAGCCGCTGTTCCTAAGTCAG-3'
F48S	5'-GCTGGTGTGTAGCCTCTGTTCCTAAGTCAG-3'
F48W	5'-GCTGGTGTGTAGCCTGGGTTCCTAAGTCAG-3'
F48Y	5'-GCTGGTGTGTAGCCTATGTTCCTAAGTCAG-3'

Determination of Iron and Sulfide Contents of the Iro Mutant Proteins

Iron assays were performed by the colorimetric method [10], and sulfide content was determined according to Siegel [15]. The samples were prepared in 20 mM phosphate buffer containing 0.5 M NaCl, pH 7.4.

Molecular Structure Modeling of the Iro Mutant Protein

The structure models for Y10A, Y10E, Y10F, Y10S, and Y10W mutant proteins were constructed using the Modeler program based on the modeled structure of the Iro protein [17]. During models generation, the structures were optimized according to CHARMM-derived stereochemical and non-bonded restraints, as well as statistical preferences for the Ramachandran plots and side-chain Rotamers of different residue types. Then, each of these initial models was carried out by the following procedures. First, they were improved by energy minimization (EM). After performing 500 steps of conjugate gradient (CG) minimization, the molecular dynamics (MD) simulations were then carried out to examine the quality of the modeled structures by 70 ps simulations at a constant temperature of 298 K. Finally, conjugate gradient energy minimizations of the full proteins were performed until the root mean square (RMS) gradient energies were lower than 0.001 kcal mol^{-1} Å^{-1}. All simulations were carried out using the Discover_3 module of the Insight II system. All the final structures were assessed by the Profile-3D and ProStat program.

RESULTS AND DISCUSSION

Expression and Purification of the Iro Mutant Proteins

A nickel metal-affinity resin column was used for single-step purifications of the mutant Iro proteins, and all the mutant proteins were obtained as soluble proteins. The purified protein fractions were dialyzed against a 20 mM potassium phosphate buffer, pH 7.4, with 5% glycerol, as soon as possible after the purification. The purities of the mutant proteins were further examined by SDS–PAGE, and single bands corresponding to the 6 kDa protein were observed with >95% purity.

The eluted Iro Y10F and Y10W mutant proteins were observed to be brown proteins, indicating that the iron–sulfur cluster is still bound to the protein after purification. The stabilities of the purified Y10F and Y10W mutant proteins were tested on the basis of their [Fe$_4$S$_4$] cluster stabilization and the mutant proteins could be stored at 4°C for one month without significant loss of the iron–sulfur cluster. The Iro Y10A, Y10E, and Y10S mutant proteins had no color after purification, indicating loss of the [Fe$_4$S$_4$] clusters. The mutant Phe26, Trp44, and Phe48 proteins were all observed to be brown proteins after purification.

CD spectra of the mutant Tyr10 proteins showed that all the mutant proteins showed similar CD spectra to that of wild-type protein, as show in Fig. 2. The results suggested that the mutant Tyr10 proteins were correctly folded and had similar secondary structures to that of wild-type protein. CD spectra of the mutant Phe26, Trp44, and Phe48 proteins were also carried out, and all the mutant proteins
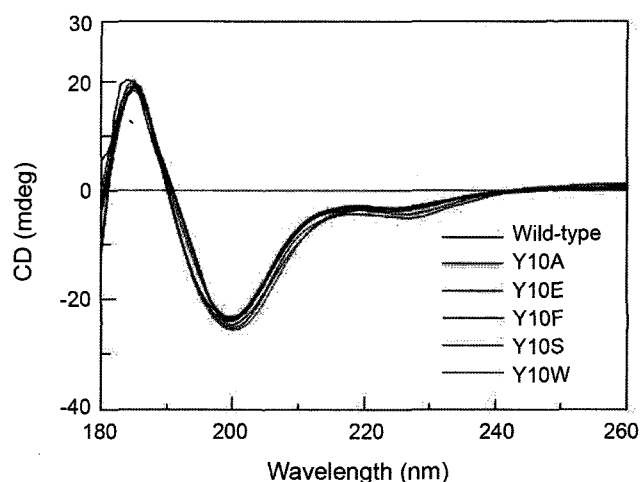
Fig. 2. CD spectra of the mutant Tyr10 proteins of the Iro protein from *A. ferrooxidans.*

showed nearly identical spectra to that of wild-type protein (data not shown), indicating that mutations of these residues had no effects on the secondary structure of the protein.

UV Scanning and EPR Spectra of the Mutant Proteins of the Iro Protein

The mutant Tyr10 proteins were then subjected to UV–Vis scanning, and the Y10F and Y10W mutant proteins after purification were observed to have a maximum visible absorption at 380 nm, as shown in Fig. 3A, which is typical for proteins containing a [Fe$_4$S$_4$] cluster [4, 5, 8, 17]. UV–Vis scanning for the Y10A, Y10E, and Y10S mutant proteins showed that there were no absorptions between 320 and 450 nm, indicating the absence of the [Fe$_4$S$_4$] clusters in the mutant proteins. The other three mutant proteins of F26A, W44A, and F48A also showed typical visible absorption at 380 nm as that of wild type, as shown in Fig. 3B, indicating that removal of the aromatic group of these residues had no effects on the stability of the iron–sulfur cluster under neutral pH.

The EPR spectra of the purified mutant Iro proteins were determined. The Iro Y10F and Y10W mutant proteins in oxidized state exhibited a typical EPR signal indicating the presence of the [Fe$_4$S$_4$]$^{3+}$ cluster. Y10A, Y10E, and Y10S mutant proteins had no EPR signal. The result further indicated that the aromatic group of the Tyr10 was essential for the stability of the [Fe$_4$S$_4$] cluster. The mutant proteins of F26A, W44A, and F48A had similar EPR signals as that of wild-type Iro protein (data not shown).

Iron and Sulfide Contents of the Mutant Proteins of the Iro Protein

The iron and sulfide contents of the Iro mutant proteins are shown in Table 2. The iron and sulfide contents for Iro Y10F and Y10W mutant proteins confirmed that both
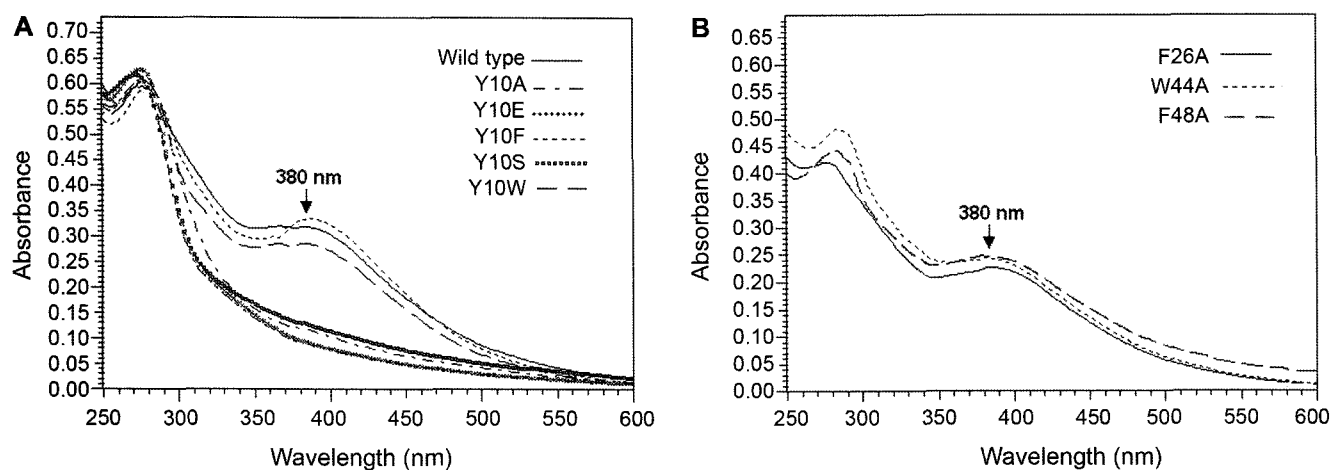
Fig. 3. **A.** UV–vis scanning of the Iro mutant Tyr10 proteins from *A. ferrooxidans*; **B.** UV–Vis scanning of the Iro F26A, W44A, and F48A mutant proteins.

The protein samples were prepared in 20 mM phosphate buffer containing 0.5 M NaCl, pH 7.4.

proteins contained a single [Fe_4S_4] cluster. The iron and sulfide contents for Iro Y10A, Y10E, and Y10S mutant proteins were all <0.5 μmol/μmol protein), indicating that the iron–sulfur cluster could not tightly bind in the proteins, and most of the [Fe_4S_4] clusters were decomposed. Mutation of Tyr10 by small or polar residues resulted in loss of the iron–sulfur cluster. The iron and sulfide contents for F26A, W44A, and F48A mutant proteins suggested that all the three mutant proteins contained a single [Fe_4S_4] cluster per molecule, and removal of the aromatic group of the three residues had no effects on the stability of the iron–sulfur cluster under neutral pH.

Roles of Tyr10, Phe26, Trp44, and Phe48 in Stabilization of the [Fe_4S_4] Cluster Under Acidic Conditions.

Tyr10 is a critical residue for the stability of the iron–sulfur cluster, but the other three residues of Phe26, Trp44, and Phe48 were not essential for the stability of the [Fe_4S_4] cluster under neutral pH. However, the Iro protein is a periplasm protein, which showed its optimal activity at pH 3.5 [16]. However, it will be interesting to study the roles

Table 2. Iron and sulfur contents of the mutant Iro proteins.

	Iron content (μmol/μmol protein)	Sulfur content (μmol/μmol protein)	Iron/sulfur
Wild type	3.77±0.10	3.80±0.09	0.99
Y10A	<0.5	<0.5	NA
Y10E	<0.5	<0.5	NA
Y10F	3.55±0.09	3.27±0.10	1.09
Y10S	<0.5	<0.5	NA
Y10W	3.21±0.09	3.43±0.10	0.94
F26A	3.46±0.07	3.71±0.09	0.93
W44A	3.59±0.10	3.24±0.09	1.11
F48A	3.81±0.08	3.66±0.07	1.04

of these residues on the stability of the iron–sulfur cluster under acidic conditions. We created mutations on these residues, and all the mutant proteins showed maximum visible absorption at 380 nm, as in that of wild type at pH 7.4, and EPR results confirmed that all the mutant proteins contained [Fe_4S_4] clusters under neutral condition. The mutant proteins were then subjected to time scanning at 380 nm under acidic conditions (pH 3.5). For the mutant Tyr10 proteins, the [Fe_4S_4] clusters in the Y10F and Y10W mutant proteins showed no significant absorption decreases under acidic condition, which were similar to the wild-type protein, as shown in Fig. 4A. For the mutant Phe26 proteins, the [Fe_4S_4] clusters in the F26A and F26S mutant proteins decomposed quickly at pH 3.5, whereas for F26W and F26Y mutant proteins, no significant absorption decreases were observed under acidic conditions, which was also similar to the wild-type protein, as shown in Fig. 4B. Similar results were observed for mutant Phe48 proteins (Fig. 4D), whereas for mutant Trp44 proteins, the iron–sulfur clusters were stable for all the mutant proteins under acidic condition, as shown in Fig. 4C. After incubating at pH 3.5 for 5 min, the mutant proteins of F26S and F48S were then subjected to wavelength scanning, and the results indicated that the two proteins after acidic treatment had no [Fe_4S_4] cluster, as shown in Fig. 4E and 4F. Hence, the results suggested that Tyr10, Phe26, and Phe48 were important residues for maintaining the stability of the [Fe_4S_4] cluster under acidic conditions. Trp44 was not involved in the stability of the iron–sulfur core.

The [Fe_4S_4] center of the Iro protein is surrounded by hydrophobic residues, of which Tyr10, Phe26, and Phe48 were found to be essential residues for maintaining the stability of the [Fe_4S_4] cluster under acidic condition. Mutation of the aromatic residues with alanine or serine will partially change the microenvironment of the binding
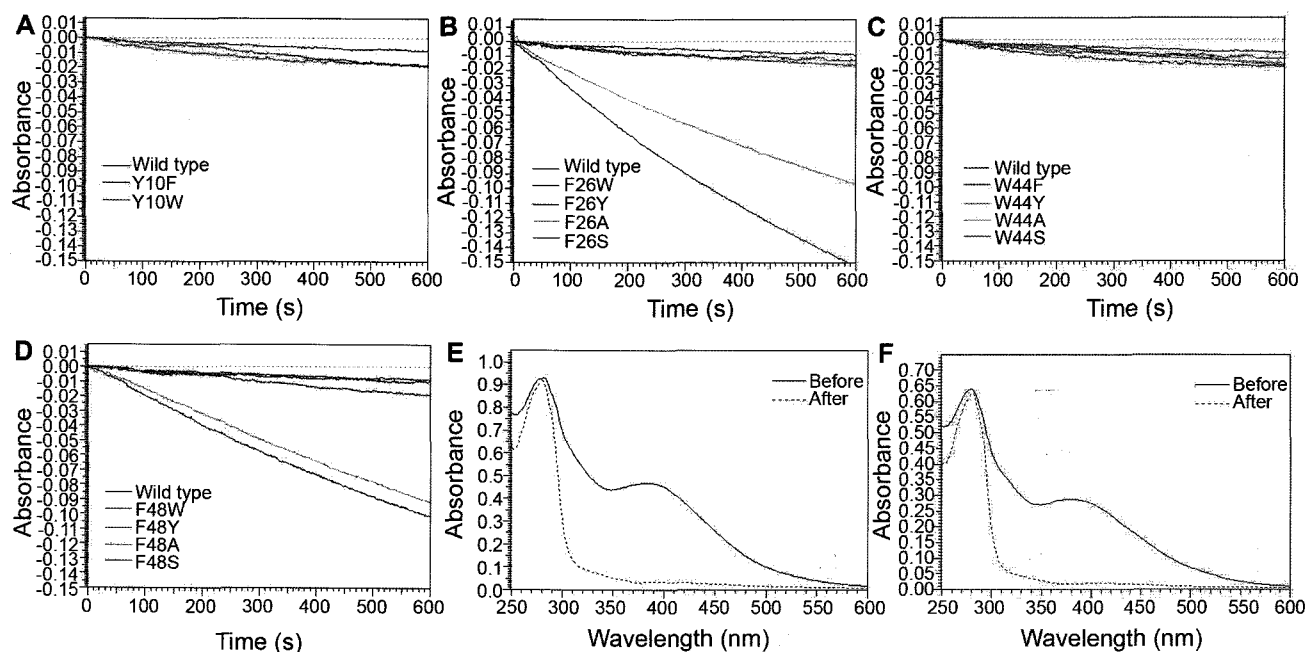
Fig. 4. A. Time course of degradation of the [Fe₄S₄] cluster in the mutant Tyr10 proteins under acidic condition; **B.** Time course of degradation of the [Fe₄S₄] cluster in the mutant Phe26 proteins under acidic condition; **C.** Time course of degradation of the [Fe₄S₄] cluster in the mutant Trp44 proteins under acidic condition; **D.** Time course of degradation of the [Fe₄S₄] cluster of the mutant Phe48 proteins under acidic condition.

The protein samples were prepared in 20 mM sodium acetate buffer, pH 3.5, and then the absorbance changes at 380 nm at 25°C were measured. **E.** Wavelength scanning of Iro F26S mutant protein before and after acidic treatment; **F.** Wavelength scanning of Iro F48S mutant protein before and after acidic treatment. The protein samples were prepared in 20 mM sodium acetate buffer, pH 3.5, and incubated at 25°C for 5 min for wavelength scanning.

pocket of the [Fe₄S₄] cluster. Therefore, the mutants cannot bind the [Fe₄S₄] cluster in the acidic environment, whereas mutations of these three residues with aromatic residues still bind the [Fe₄S₄] cluster under acidic condition since the mutant proteins still have aromatic groups that protect the [Fe₄S₄] center from acidic hydrolysis.

Molecular Structure Modeling of the Iro Mutant Tyr10 Proteins

All the obtained structures were accessed by the ProStat program, and no significant differences of structure features in the modeled proteins were observed. When the obtained structures were checked by the Profile-3D program, the compatibility scores for each residue in all of the structures were all above zero, which corresponded to acceptable side-chain environments. The above results from the Profile-3D and ProStat programs confirmed that the modeled structures were reliable.

The modeled overall structure of the Iro protein wild type is shown in Fig. 5A. The [Fe₄S₄] cluster was located in the center of the protein, which was ligated by four highly conserved cysteine residues, Cys20, Cys23, Cys32, and Cys45 [13]. The [Fe₄S₄] was surrounded by four aromatic residues of Tyr10, Phe26, Trp44, and Phe48, and the aromatic residues surrounding the iron–sulfur cluster were commonly found in the HiPIP family, which were

proposed to be responsible for the stability of the [Fe₄S₄] cluster in previous reports [2, 7, 11, 12, 14]. Our results by site-directed mutagenesis indicated that Tyr10 was a critical aromatic residue responsible for the stability of the [Fe₄S₄] cluster. Phe26 and Phe48 were proposed to be in the external surface of the hydrophobic area surrounding the iron–sulfur core, maintaining the acidic stability of the [Fe₄S₄] cluster. Trp44 might be buried in the hydrophobic area and was not directly involved in maintaining the stability of the protein. The location of the aromatic residues of the Iro protein might be different from that of HiPIPs in previous reports [2, 7, 11, 14], and further researches including structure resolution for the Iro protein will be carried out to explain the difference.

The modeled structures for Iro Y10F and Y10W mutant proteins revealed that substitution of tyrosine by aromatic residues resulted in no significant conformational changes compared with that of the wild-type protein, as shown in Fig. 5B. The solvent could not enter into the cluster cavity, so the [Fe₄S₄] cluster was stable. For the Y10A, Y10E, and Y10S mutant proteins, the modeled structures showed that the [Fe₄S₄] clusters were all open to the outer environment, and replacement of Tyr10 by a small or polar residue resulted in a significant perturbation of the polarity of one side of the cluster cavity, which allowed a greater degree of solvent accessibility compared with wild-type Iro protein.
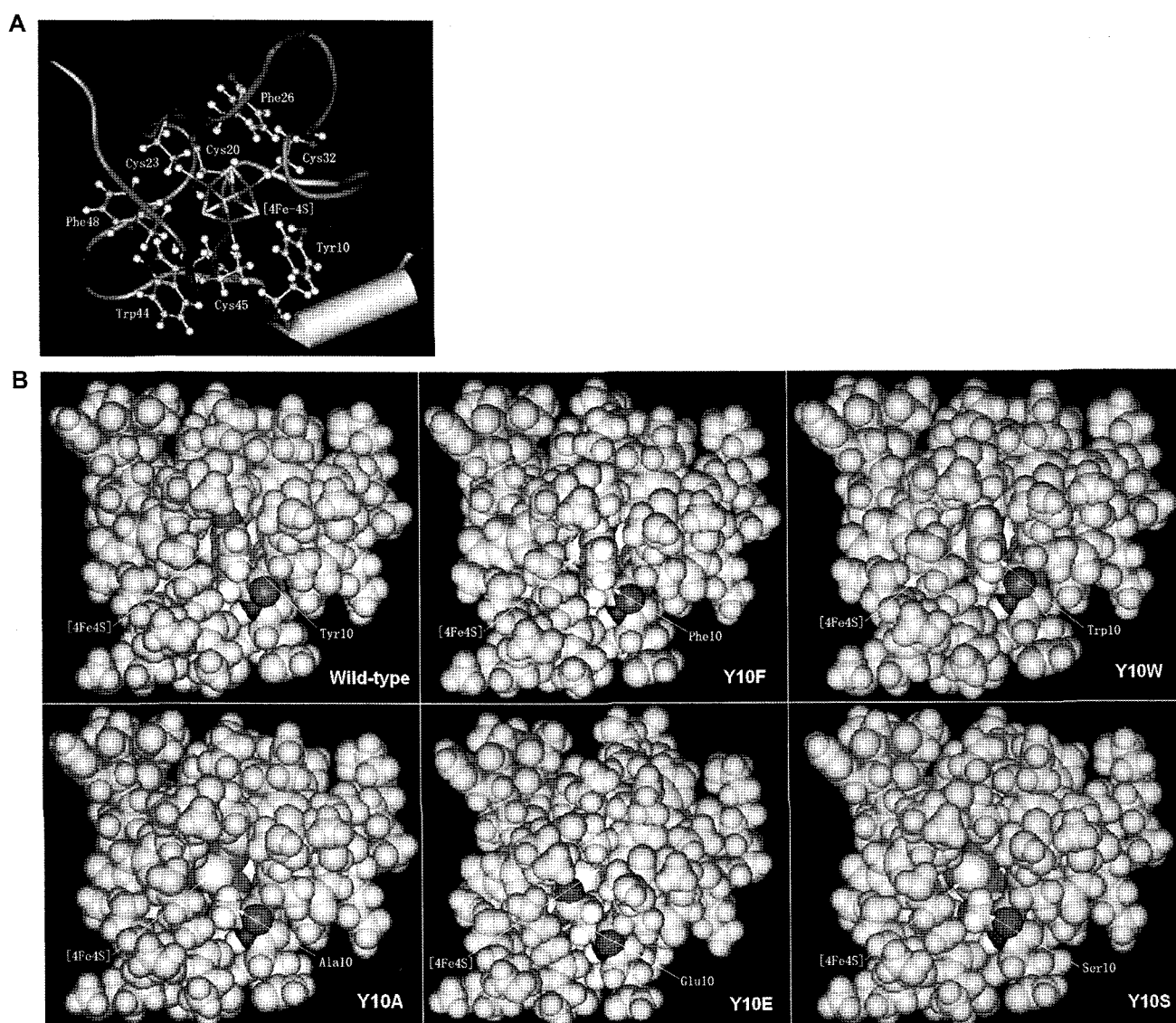
A

B

Fig. 5. A. The modeled structure of the Iro protein from *A. ferrooxidans* [17], where the [Fe₄S₄] cluster is shown by purple-yellow sticks **B.** The modeled structures for mutant Tyr10 proteins, where the [Fe₄S₄] cluster is shown by purple-yellow balls buried in the cluster cavity.

Solvent accessibility resulted in more facile oxidation of the cluster by dioxygen, with subsequent rapid hydrolysis of the [Fe₄S₄] cluster (Fig. 5B).

Abbreviations

Abbreviations used are as follows: *A. ferrooxidans*, *Acidithiobacillus ferrooxidans*; HiPIP, high redox potential iron–sulfur proteins; IPTG, isopropyl-D-thiogalactopyranoside; PAGE, polyacrylamide gel electrophoresis; PCR, polymerase chain reaction; SDS, sodium dodecyl sulfate; EPR, electronic paramagnetic resonance.

Acknowledgments

REFERENCES

1. Agarwal, A., D. Li, and J. A. Cowan. 1995. Role of aromatic residues in stabilization of the [Fe₄S₄] cluster in high-potential

Iro proteins (HiPIPs): Physical characterization and stability studies of Tyr-19 mutants of *Chromatium vinosum* HiPIP. *Proc. Natl. Acad. Sci. U.S.A.* **92**: 9440–9444.

2. Banci, L., I. Bertini, A. Dikiy, D. H. Kastrau, C. Luchinat, and P. Sompornpisut. 1995. The three-dimensional solution structure of the reduced high-potential iron–sulfur protein from *Chromatium vinosum* through NMR. *Biochemistry* **34**: 206–219.

3. Bradford, M. M. 1976. A rapid and sensitive method for the quantitation of microgram quantities of protein utilizing the principle of protein-dye binding. *Anal. Biochem.* **72**: 248–254.

4. Cavazza, C., B. Guigliarelli, P. Bertrand, and M. Bruschi. 1995. Biochemical and EPR characterization of a high potential iron–sulfur protein in *Thiobacillus ferrooxidans*. *FEMS Microbiol. Lett.* **130**: 193–200.

5. Fukumori, Y., T. Yano, A. Sato, and T. Yamanaka. 1988. Fe(II)-oxidizing enzyme purified from *Thiobacillus ferrooxidans*. *FEMS Microbiol. Lett.* **50**: 169–172.

6. Iwagami, S. G., A. L. Creagh, C. A. Haynes, M. Borsari, I. C. Felli, M. Piccioli, and L. D. Eltis. 1995. The role of a conserved tyrosine residue in high-potential iron–sulfur proteins. *Protein Sci.* **4**: 2562–2572.

7. Kerfeld, C. A., A. E. Salmeen, and T. O. Yeates. 1998. Crystal structure and possible dimerization of the high-potential iron–sulfur protein from *Chromatium purpuratum*. *Biochemistry* **37**: 13911–13917.

8. Kusano, T., T. Takeshima, K. Sugawara, C. Inoue, T. Shiratori, T. Yano, Y. Fukumori, and T. Yamanaka. 1992. Molecular cloning of the gene encoding *Thiobacillus ferrooxidans* Fe(II) oxidase. High homology of the gene product with HiPIP. *J. Biol. Chem.* **267**: 11242–11247.

9. Laemmli, U. 1970. Cleavage of structural proteins during the assembly of the head of bacteriophage T4. *Nature* **227**: 680–685.

10. Lovenberg, W., B. B. Buchanan, and J. C. Rabinowitz. 1963. Studies on the chemical nature of clostridial ferredoxin. *J. Biol. Chem.* **238**: 3899–3913.

11. Mansy, S. S., Y. Xiong, C. Hemann, R. Hille, M. Sundaralingam, and J. A. Cowan. 2002. Crystal structure and stability studies of C77S HiPIP: A serine ligated [4Fe–4S] cluster. *Biochemistry* **41**: 1195–1201.

12. Nouailler, M., P. Bruscella, E. Lojou, R. Lebrun, V. Bonnefoy, and F. Guerlesquin. 2006. Structural analysis of the HiPIP from the acidophilic bacteria: *Acidithiobacillus ferrooxidans*. *Extremophiles* **10**: 191–198.

13. Rawlings, D. E. 2001. The molecular genetics of *Thiobacillus ferrooxidans* and other mesophilic, acidophilic, chemolithotrophic, iron- or sulfur-oxidizing bacteria. *Hydrometallurgy* **59**: 187–201.

14. Rayment, I., G. Wesenberg, T. E. Meyer, M. A. Cusanovich, and H. M. Holden. 1992. Three-dimensional structure of the high-potential iron–sulfur protein isolated from the purple phototrophic bacterium *Rhodocyclus tenuis* determined and refined at 1.5 Å resolution. *J. Mol. Biol.* **228**: 672–686.

15. Siegel, L. M. 1965. A direct microdetermination for sulfide. *Anal. Biochem.* **11**: 126–132.

16. Yamanaka, T. and Y. Fukumori. 1995. Molecular aspects of the electron transfer system which participates in the oxidation of ferrous ion by *Thiobacillus ferrooxidans*. *FEMS Microbiol. Rev.* **17**: 401–413.

17. Zeng, J., M. Geng, Y. Liu, W. Zhao, L. Xia, J. Liu, and G. Qiu. 2007. Expression, purification and molecular modeling of the Iro protein from *Acidithiobacillus ferrooxidans* Fe-1. *Protein Expr. Purif.* **52**: 146–152.